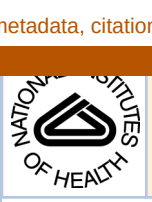

Published in final edited form as:

Nat Biotechnol. 2010 March ; 28(3): 264–270. doi:10.1038/nbt.1609.

Directed evolution of a magnetic resonance imaging contrast agent for noninvasive imaging of dopamine

Mikhail G Shapiro[1,5], **Gil G Westmeyer**[2,5], **Philip A Romero**[3], **Jerzy O Szablowski**[1], **Benedict Küster**[2], **Ameer Shah**[1], **Christopher R Otey**[3], **Robert Langer**[1], **Frances H Arnold**[3], and **Alan Jasanoff**[1,2,4]

[1] Department of Biological Engineering, Massachusetts Institute of Technology, Cambridge, Massachusetts, USA

[2] Department of Brain & Cognitive Sciences, Massachusetts Institute of Technology, Cambridge, Massachusetts, USA

[3] Division of Chemistry & Chemical Engineering, California Institute of Technology, Pasadena, California, USA

[4] Department of Nuclear Science & Engineering, Massachusetts Institute of Technology, Cambridge, Massachusetts, USA

Abstract

The development of molecular probes that allow *in vivo* imaging of neural signaling processes with high temporal and spatial resolution remains challenging. Here we applied directed evolution techniques to create magnetic resonance imaging (MRI) contrast agents sensitive to the neurotransmitter dopamine. The sensors were derived from the heme domain of the bacterial cytochrome P450-BM3 (BM3h). Ligand binding to a site near BM3h's paramagnetic heme iron led to a drop in MRI signal enhancement and a shift in optical absorbance. Using an absorbance-based screen, we evolved the specificity of BM3h away from its natural ligand and toward dopamine, producing sensors with dissociation constants for dopamine of 3.3–8.9 μM. These molecules were used to image depolarization-triggered neurotransmitter release from PC12 cells and in the brains of live animals. Our results demonstrate the feasibility of molecular-level functional MRI using neural activity–dependent sensors, and our protein engineering approach can be generalized to create probes for other targets.

MRI is a uniquely valuable tool for studying the brain because MRI scans are noninvasive and can provide information at relatively high spatial resolution (< 100 μm) and temporal

Correspondence should be addressed to A.J. (jasanoff@mit.edu).

[5]These authors contributed equally to this work.

Note: Supplementary information is available on the Nature Biotechnology website.

AUTHOR CONTRIBUTIONS

M.G.S. conceived and performed the directed evolution and *in vitro* assessment of dopamine sensors; G.G.W. designed and conducted the *in vivo* experiments; P.A.R. performed directed evolution screening for BM3h variants; J.O.S. assisted with screening and *in vitro* experiments; B.K. assisted with data analysis for *in vivo* experiments; A.S. assisted with *in vivo* experiments; C.R.O. worked with M.G.S. to establish BM3h screening methods; R.L. provided consultation and essential materials; F.H.A. supervised the directed evolution work; A.J. established research direction, supervised the project overall and co-wrote the paper with M.G.S. and G.G.W.

COMPETING INTERESTS STATEMENT

The authors declare no competing financial interests.

resolution (~1 s) from living specimens. Functional imaging (fMRI) of brain activity is possible with MRI methods sensitive to cerebral hemodynamics[1]. The most common fMRI technique, blood oxygen level–dependent (BOLD) fMRI, is based on oxygenation of hemoglobin, an endogenous oxygen-sensitive MRI contrast agent present in the blood[2]. Although BOLD fMRI has had a tremendous impact in neuroscience, the method provides only a slow and indirect readout of neural activity, owing to the complexity of neurovascular coupling[3]. Considerably more precise measurements of brain function would be possible with MRI sensors that were directly and rapidly responsive to neurochemicals involved in the brain's information processing[4].

The challenging process of developing sensors for next-generation neuroimaging could be greatly accelerated using advanced molecular engineering techniques. Directed evolution is a molecular engineering method that employs successive rounds of mutagenesis and selection to generate proteins with novel functionality, starting from a molecule with some of the desired properties of the end product[5]. This technique could be applied to evolve MRI sensors from proteins that are magnetically active (for example, paramagnetic) and have tunable ligand-binding or catalytic properties.

The flavocytochrome P450-BM3 (BM3), a fatty acid hydroxylase from *Bacillus megaterium*, contains a paramagnetic iron atom embedded in a solvent-accessible substrate-binding pocket, suggesting that it could produce ligand-dependent MRI signal changes. BM3's binding specificity is also highly tunable, as demonstrated by previous efforts to identify novel enzymatic activities through directed evolution of this protein[6–9]. If BM3 variants could be engineered to act as MRI sensors, they would be genetically encodable, an added advantage over synthetic molecular imaging agents.

We sought to apply directed evolution of BM3 to develop MRI sensors for a key signaling molecule in the brain, the neurotransmitter dopamine. To our knowledge, no MRI contrast agent for sensing dopamine (or any other neurotransmitter) currently exists, but there is considerable interest in measuring dopamine-related activity by MRI[10]. Dopamine is of particular significance because of its roles in learning, reward and motor coordination[11], and because the dysfunction of dopaminergic systems underlies addiction[12] and several neurodegenerative diseases[13]. Existing techniques for measuring dopamine *in vivo* are either invasive point-measurement methods[14–16] or positron emission tomography procedures[17] with low spatial and temporal resolution. MRI could be used successfully for dopamine measurement if combined with an imaging agent capable of responding quickly, reversibly and specifically to extracellular dopamine fluctuations from <1 μM to tens of micromolar[18,19]. To be comparable with established functional brain imaging techniques, interaction of dopamine with the probe should also produce image signal changes on the order of 1% or more *in vivo*[20]. Here we show that directed evolution of BM3 is capable of producing dopamine sensors that largely meet these specifications.

RESULTS

P450 BM3 reports ligand binding in MRI

To evolve dopamine probes for MRI, we focused on the heme domain of BM3 (BM3h), a 53-kDa moiety that is catalytically inactive in the absence of the full protein's reductase domain[21]. BM3h contains a single iron(III) atom (mixed spin 1/2 and 5/2)[22] bound to a hemin prosthetic group and axially coordinated by residue Cys400 on the protein. In the absence of substrates, the remaining coordination site is filled by a water molecule[23]. Interaction of the heme iron with exchanging water molecules at this axial site promotes T_1 relaxation in aqueous solutions[24] and is therefore predicted to modulate MRI contrast. To determine the extent of this effect, we used a spin echo pulse sequence in a 4.7-T MRI

scanner to measure the proton relaxation rate as a function of protein concentration in PBS; the slope of this relationship (T_1 relaxivity, or r_1) provides a standard measure of the strength of a contrast agent. For BM3h in the absence of ligands, an r_1 value of 1.23 ± 0.07 mM^{-1} s^{-1} was obtained. Addition of a saturating quantity of the natural BM3 substrate, arachidonic acid (400 μM concentration), resulted in an r_1 of 0.42 ± 0.05 mM^{-1} s^{-1} (Fig. 1a). This ligand-induced decrease in relaxivity, probably arising from the displacement of water molecules at the BM3h heme, enabled quantitative sensing of arachidonic acid using MRI (Fig. 1b) and suggested that BM3h could serve as a platform for molecular sensor engineering.

We next tested whether dopamine or related compounds could serve as unnatural ligands to BM3h when applied at high enough concentrations. As measured by MRI, addition of 1 mM dopamine to BM3h in fact induced a drop in r_1 to 0.76 ± 0.03 mM^{-1} s^{-1} (Fig. 1a). Binding of arachidonic acid is known to induce a change (blue shift) in BM3h's optical absorbance spectrum because of perturbation of the electronic environment of the heme chromophore[25]. To determine whether the relaxation change induced by dopamine also reflects interaction with the BM3h heme, we measured optical spectra of the protein in the presence and absence of 1 mM dopamine. The interaction produced a small but clearly discernable red shift of λ_{max}, from 419 to 422 nm (Fig. 1c), indicative of ligand coordination to the heme iron[25]. This suggests that dopamine (at 1 mM) directly replaces water as an axial metal ligand in the BM3h substrate-binding pocket and that directed evolution of BM3h binding specificity could therefore improve the protein's relative affinity for dopamine. In addition to providing mechanistic insight, the correspondence between optical and MRI measurements of ligand binding to BM3h implied that either modality could be used to obtain quantitative binding parameters. We monitored the difference between absorption at two wavelengths as a function of ligand concentration to determine binding isotherms for arachidonic acid and dopamine (Fig. 1d,e). For BM3h, the apparent K_d for arachidonic acid was 6.8 ± 0.5 μM; the K_d for dopamine was 990 ± 110 μM. Goals for the production of BM3h-based MRI sensors thus included decreasing the affinity for arachidonic acid, increasing the dopamine affinity by at least two orders of magnitude and maintaining or enhancing the relaxivity changes observed upon ligand binding.

Directed evolution of dopamine-responsive BM3h variants

To create an MRI sensor for dopamine using directed evolution, we developed a customized screening methodology (Fig. 2a). Results shown in Figure 1 suggested that either MRI-based or optical assays could be used to distinguish BM3h mutants with differing ligand affinities. We chose an absorbance assay for our screen because lower protein concentrations (~1 μM) could be used in this format. Input to each round of screening consisted of a library of BM3h mutants, each with an average of one to two amino acid substitutions, generated by error-prone PCR from the wild-type (WT) gene or a previously selected mutant. We transformed DNA libraries into *Escherichia coli*. We grew and induced approximately 900 randomly selected clones in microtiter plate format, then prepared cleared lysates for optical titration with dopamine and arachidonic acid in a plate reader. Titration data were analyzed to determine K_d values for both ligands. An average of 79% of assayed mutants had sufficient protein levels (absorbance signal > 30% of parent) and clean enough titration curves ($r^2 > 0.8$) for K_d estimation. Mutant affinities appeared to be distributed randomly about the dissociation constant measured for the corresponding parent protein, but we were able to identify individual clones with desired affinity changes in each round (Fig. 2b). From each screen, we chose eight to ten mutants on the basis of their estimated K_ds, purified them in bulk, retitrated them to obtain more accurate estimates of their dopamine and arachidonic acid affinities, and examined them with MRI to ensure that robust ligand-induced changes in r_1 could be detected. On the basis of these assays, we

chose as a parent for the next round of evolution the mutant showing the best combination of relaxivity changes, improved dopamine affinity and decreased affinity for arachidonic acid.

After carrying out the screening strategy over multiple rounds, we found a steady trend in the distribution of K_d values toward greater affinity for dopamine and less affinity for arachidonic acid (Fig. 2b–d). Little change in binding cooperativity was observed, and changes in partial saturation generally occurred over 100-fold ranges of dopamine concentrations. Five rounds of evolution yielded a BM3h variant with eight mutations (Fig. 2e), four near the ligand-binding pocket and four at distal surfaces of the protein. One residue (Ile263) was first mutated to threonine (third round), then to alanine (fourth round). The clones selected from rounds 1, 3 and 5 had two new mutations each. We did not determine the individual contributions of these mutations to the observed changes in affinity. We introduced the mutation I366V by site-directed mutagenesis before the fifth round to enhance thermostability and tolerance of BM3h to further mutation[26,27]; it did not noticeably affect dopamine binding affinity.

The mutant proteins selected after the fourth and fifth rounds of evolution, denoted BM3h-8C8 and BM3h-B7, had optically determined dissociation constants of 8.9 ± 0.7 μM and 3.3 ± 0.1 μM, respectively, for dopamine, and 750 ± 140 μM and 660 ± 80 μM, respectively, for arachidonic acid. The T_1 relaxivity of BM3h-8C8 was 1.1 ± 0.1 mM^{-1} s^{-1} in the absence of ligand and 0.17 ± 0.03 mM^{-1} s^{-1} in the presence of 400 μM dopamine (Fig. 3a). For BM3h-B7, the corresponding r_1 values were 0.96 ± 0.13 mM^{-1} s^{-1} and 0.14 ± 0.04 mM^{-1} s^{-1}. Both sensor variants showed a dopamine concentration–dependent decrease in T_1-weighted MRI signal (up to 13% with 28.5 μM protein) that could be fitted by binding isotherms with estimated K_d values of 4.9 ± 2.7 μM for BM3h-8C8 and 2.7 ± 2.9 μM for BM3h-B7 (Fig. 3b,c). For both BM3h variants, the stability, reversibility and rate of dopamine binding were established using spectroscopic assays (Supplementary Figs. 1 and 2).

We investigated the reporting specificities of BM3h-8C8 and BM3h-B7 for dopamine by measuring MRI signal changes that resulted from incubation of 28.5 μM of each protein with 30 μM of either dopamine or one of eight other neuroactive molecules: norepinephrine (a neurotransmitter formed by catalytic hydroxylation of dopamine), 3,4-dihydroxy-L-phenylalanine (DOPA, the biosynthetic precursor to dopamine), serotonin, glutamate, glycine, γ-aminobutyric acid (GABA), acetylcholine and arachidonic acid (Fig. 3d). Of these potential ligands, only dopamine, norepinephrine and serotonin elicited substantial changes in the T_1 relaxation rate ($1/T_1$). For BM3h-8C8, the $1/T_1$ reductions produced by norepinephrine and serotonin were 0.0076 ± 0.0023 s^{-1} and 0.0041 ± 0.0020 s^{-1}, respectively, compared to 0.0182 ± 0.0006 s^{-1} for dopamine; for BM3h-B7, norepinephrine and serotonin induced $1/T_1$ decreases of 0.0112 ± 0.0024 s^{-1} and 0.0171 ± 0.0005 s^{-1}, respectively, compared to 0.0208 ± 0.0002 s^{-1} for dopamine. We measured the affinities of BM3h-based dopamine sensors for these competitors spectroscopically (Fig. 3d, inset). For BM3h-8C8, measured K_ds were 44 ± 3 μM and 80 ± 8 μM for norepinephrine and serotonin, respectively, and for BM3h-B7 the K_d values were 18.6 ± 0.4 μM and 11.8 ± 0.1 μM, respectively. Although both BM3h-8C8 and BM3h-B7 show substantially higher affinity for dopamine than for norepinephrine (fivefold and sixfold, respectively) or for serotonin (ninefold and fourfold, respectively), the BM3h-8C8 variant is more specific for sensing dopamine at concentrations above 10 μM. In settings where dopamine is known to be the dominant neurotransmitter, BM3h-B7 may provide greater overall sensitivity.

The specificity data also provided a possible indication of the geometry of dopamine binding to the evolved BM3h proteins. Only monoamines showed affinity for BM3h-8C8 and BM3h-B7, whereas two catechols that lack primary amines, epinephrine and 3,4-

dihydrophenylacetic acid, showed no measurable affinity (data not shown). Combined with the spectral evidence that dopamine directly coordinates the BM3h heme (Fig. 1c), the titration results therefore suggest that the dopamine amine may serve as an axial ligand to the BM3h heme in the sensor-analyte complexes we examined.

BM3h-based sensors detect dopamine released from PC12 cells

We asked whether BM3h mutants produced by directed evolution could sense dopamine release in a standard cellular model of dopaminergic function. We applied an established protocol[28] to test the ability of our sensors to measure dopamine discharge from PC12 cells stimulated with extracellular K^+ (Fig. 4a). Cells were cultured in serum-free medium supplemented with dopamine to promote packaging of the neurotransmitter into vesicles. After pelleting and washing, we resuspended cells in a physiological buffer containing 32 μM BM3h-B7 and either 5.6 or 59.6 mM K^+ (cells in the low-K^+ condition were osmotically balanced with Na^+). T_1-weighted MRI images (spin echo TE/TR = 10/477 ms) obtained with BM3h-B7 showed a 4.0 ± 0.5% reduction in signal intensity in the supernatant of K^+-stimulated cells, compared with cells for which isotonic Na^+ was used as control (Fig. 4b). This corresponded to a 54 ± 4% decrease in sensor r_1 (Fig. 4c). Given the dopamine dissociation constant of BM3h-B7 and its relaxivities under ligand-free and dopamine-saturated conditions, and assuming negligible dilution of the sensor after mixing with cells, we estimated supernatant dopamine concentrations of 60.3 ± 7.9 μM for stimulated cells and 22.2 ± 1.1 μM for controls. These estimates were in reasonable agreement with an independent quantification of dopamine release measured using an enzyme-linked immunosorbent assay (ELISA), which yielded concentrations of 54 ± 9 μM and 13 ± 2 μM for stimulated and control cells, respectively (Fig. 4d). We were also able to use BM3h-8C8 to image dopamine release from PC12 cells. Under experimental conditions similar to above, BM3h-8C8 had a 37 ± 2% reduction in r_1 in the supernatant of K^+-stimulated cells relative to Na^+ controls (Supplementary Fig. 3).

Dopamine detection in the brain of living rats

As an initial test of the ability of BM3h-based sensors to measure dopamine concentrations in intact animals, we injected BM3h-8C8 in the presence or absence of exogenous dopamine into the brains of anesthetized rats. We chose this simple experimental protocol for validation of the sensor because it guaranteed the presence of reproducible and unambiguous micromolar-level dopamine concentrations, suitable for evoking robust responses from our sensors *in vivo*. We obtained T_1-weighted MRI scans (fast spin echo TE/TR 14/277 ms, 8.9 s per image) continuously during 0.5-μl-min^{-1} paired infusions of 500 μM BM3h-8C8 with and without 500 μM dopamine, via cannulae implanted stereotaxically into the left and right striatum. Dopamine-dependent contrast changes were apparent in images obtained during and after the injection period (Fig. 5a). We quantified MRI changes across multiple trials in striatal regions of interest (ROIs) that were reliably (though inhomogeneously) filled by convective spread of the contrast agent from the cannula tips (~1.5 mm radius). Consistent with results obtained *in vitro*, a of dopamine dampened the observed MRI intensity enhancement by approximately 50% (Fig. 5b); the effect was significant (*t*-test, $P = 0.003$, $n = 7$). We performed the same paired infusion procedure with WT BM3h, which has very low affinity for dopamine (K_d ~1 mM). As expected, the time course of the MRI signal during and after the WT BM3h injection period (Fig. 5c) was not significantly affected by the presence or absence of dopamine (*t*-test, $P = 0.8$, $n = 5$), indicating that the dopamine-dependent signal differences shown in Figure 5b require the presence of a micromolar-affinity dopamine sensor and cannot be explained by physiological or biochemical effects of dopamine itself. Moreover, infusion of 500 μM dopamine alone into the brain produced no noticeable signal changes in an equivalent experiment (data not shown). Histological analysis showed minimal evidence of toxicity due to these procedures (Supplementary Fig.

4). Using relaxivity values measured for BM3h-8C8 *in vitro*, we estimated maximal concentrations of 89 ± 19 μM BM3h-8C8 and 75 ± 28 μM dopamine from the data of Figure 5b, averaged across the striatal ROIs. The ability to quantify BM3h-8C8 concentration on the basis of its T_1 enhancement in the absence of elevated dopamine represents an advantage of this sensor's 'turn-off' mechanism.

To test whether BM3h-8C8 could detect release of endogenous neuro-transmitters in the rat brain, we acquired MRI data during co-infusion of the dopamine sensor with elevated concentrations of K^+, a depolarizing chemical stimulus shown previously to release large amounts of dopamine into the striatum[29,30]. We chose K^+ over pharmacological stimuli to obviate potential solubility- or viscosity-related artifacts in the experimental paradigm. K^+ itself had no effect on r_1 of the BM3h variants (data not shown). In the stimulation experiments, three 5-min blocks of high-K^+ (153 mM) infusion alternated with 10-min 'rest' periods during which we administered a low-K^+ solution (3 mM, osmotically balanced with Na^+). Both high- and low-K^+ solutions were delivered at a rate of 0.2 μl min^{-1} and also contained 500 μM BM3h-8C8, ensuring that a relatively constant concentration of dopamine sensor was present through-out the procedure. We acquired T_1-weighted MRI scans continuously as for the exogenous dopamine infusion experiments. To control for effects unrelated to neurotransmitter sensing by the contrast agent (potentially including K^+-induced edema or hemodynamic responses incompletely suppressed by the T_1-weighted spin echo pulse sequence), we paired each striatal injection of BM3h-8C8 with an injection of WT BM3h into the opposite hemisphere, following the same blocked K^+ stimulation paradigm for both injections. As in conventional 'block design' fMRI, we performed a *t*-test analysis to evaluate the correspondence of each voxel's intensity time course with the alternating periods of low and high K^+. We determined an appropriate temporal shift for the stimulus-related analysis windows with respect to infusion buffer switches by observing the time courses of similarly switched mock infusions into 0.6% agarose phantoms[31] and by comparing these with statistical results as a function of offset (Supplementary Fig. 5 and Online Methods). As additional controls for MRI effects unrelated to dopamine sensing, we examined MRI signal change in response to K^+ stimulation and again in response to dopamine infusion, both in the absence of contrast agents (data not shown). We also continuously monitored blood oxygen levels and heart rate. In no case were stimulus-associated changes observed.

Figure 5d shows the distribution of voxels with significant (*t*-test, $P < 0.01$) MRI signal decreases in response to K^+ stimulation in a single rat. We performed a group analysis by combining data from all subjects ($n = 6$) over geometrically defined ROIs centered around the injection cannula tips in each animal. In three slices spanning the infusion site, seven voxels within 0.75 mm of the BM3h-8C8 injection cannula, but only one voxel near the WT cannula, showed strong correlation ($P < 0.01$) with the stimulus. We mapped mean signal decreases over 2.7-mm-diameter ROIs corresponding to the BM3h-8C8 and WT BM3h injection sites in the group analysis (Fig. 5e). Again, dopamine sensor–dependent responses were apparent. The signal difference between low- and high-K^+ periods averaged across the entire BM3h-8C8 ROI (all voxels within a 2.7-mm-diameter by 3-mm-long cylinder, regardless of modulation by K^+) was 0.07%, whereas the signal difference averaged across the control ROI was −0.02% (Fig. 5f). The high- versus low-K^+ signal difference observed near the BM3h-8C8 infusion site was significant (*t*-test, $P = 0.0008$) and consistent with the expected suppression of MRI signal by dopamine release under high-K^+ conditions.

The mean time course of all stimulus-correlated voxels ($P < 0.05$) showing K^+-induced MRI signal changes near the BM3h-8C8 injection site, averaged over animals, is shown in Figure 5g. Discernable signal decreases of up to 3% were produced during each K^+ stimulation block. The first K^+ block evoked the largest response (presumably because of partial

dopamine depletion over subsequent blocks[32]) and elicited a clear spatiotemporal pattern of mean MRI signal change from baseline over the course of the stimulation period (Fig. 5g, top panels).

DISCUSSION

These results demonstrate the feasibility of developing molecular-level fMRI sensors and serve as a proof of principle that BM3h-based probes can be used to monitor dopamine signaling processes *in vivo*. With the experimental conditions and estimated sensor concentrations (34 ± 4 μM) used for our K^+ stimulation experiments, MRI signal changes of ~3% would be evoked by the rewarding brain stimuli reported in previous studies to release large amounts of dopamine[18,19]. This amplitude is reasonably large by functional imaging standards, and it could be used in the near term to map phasic dopamine release at high resolution across the striatum, or more generally to study mesolimbic dopamine dynamics in animal models of reward processing and neurological conditions that can be probed with strong stimuli.

Sensitivity gains will be possible using repeated stimulation and statistical analysis techniques, as in conventional fMRI, and by optimizing the imaging approach itself. For instance, higher-field scanners and faster alternatives to the T_1-weighted spin echo pulse sequences we used here may offer improved signal-to-noise ratios. Directed evolution or rational modification of BM3h variants for substantially higher relaxivity is possible as well (unpublished data). Sensors with higher relaxivity will produce larger MRI signal changes, and could have the added benefit of reducing the potential for dopamine buffering, because they may be used at lower concentrations *in vivo*: with 35 μM sensor and 35 μM total dopamine present, for example, ~60% of the dopamine would be bound to the sensor, but with 15 μM sensor present, only ~30% dopamine would be sequestered. Protein engineering techniques could also be used to improve the dopamine affinity and specificity of the first-generation sensors described here.

Our method for producing dopamine sensors represents a general paradigm for the development of molecular probes for MRI. Sensors may be evolved for targets inside or outside the brain; the diversity of potential targets is exemplified by the contrast between WT BM3h, which produces MRI signal changes in response to long-chain fatty acids, and BM3h-8C8 and BM3h-B7, which respond to a catecholamine. Contrast agents engineered to detect dopamine and other signaling molecules in the brain will permit functional neuroimaging based on direct detection of neuronal events rather than hemodynamic changes. Exogenous delivery of macromolecules such as BM3h to large regions of animal brains should be possible using a variety of techniques[33]. Because BM3h is a protein, it might also be possible to deliver variants via expression from transfected cells *in vivo* or in transgenic subjects. Preliminary evidence that BM3h can be expressed to 1% protein content in mammalian cells supports the feasibility of this approach (Supplementary Results). Because of their small size, BM3h-based dopamine sensors might sample synaptic dopamine better than voltammetry or microdialysis probes, and with appropriate targeting could potentially become synapse specific. Dopamine sensor-dependent MRI would offer a combination of spatial coverage and precision inaccessible to other methods and uniquely suited to studies of dopaminergic function in systems neuroscience research.

METHODS

Methods and any associated references are available in the online version of the paper at http://www.nature.com/naturebiotechnology/.

Supplementary Material

Refer to Web version on PubMed Central for supplementary material.

Acknowledgments

We thank V. Lelyveld for helpful discussions and assistance with *in vitro* measurements, N. Shah for help with MRI procedures and W. Schulze for help with automated analysis methods. We are grateful to C. Jennings and D. Cory for comments and suggestions about the manuscript, and to D. Vaughan for consultation regarding histology. We thank P. Caravan and again D. Cory for access to low-field relaxometers. M.G.S. thanks the Fannie and John Hertz Foundation and the Paul and Daisy Soros Fellowship for generous support. This work was funded by a Dana Foundation Brain & Immuno-Imaging grant, a Raymond & Beverley Sackler Fellowship and US National Institutes of Health (NIH) grants R01-DA28299 and DP2-OD2441 (New Innovator Award) to A.J., NIH grant R01-GM068664 and a grant from the Caltech Jacobs Institute for Molecular Medicine to F.H.A. and NIH grant R01-DE013023 to R.L.

References

1. Buxton, RB. Introduction to Functional Magnetic Resonance Imaging: Principles and Techniques. Cambridge University Press; New York: 2001.
2. Ogawa S, Lee TM, Kay AR, Tank DW. Brain magnetic resonance imaging with contrast dependent on blood oxygenation. Proc Natl Acad Sci USA. 1990; 87:9868–9872. [PubMed: 2124706]
3. Logothetis NK. What we can do and what we cannot do with fMRI. Nature. 2008; 453:869–878. [PubMed: 18548064]
4. Jasanoff A. MRI contrast agents for functional molecular imaging of brain activity. Curr Opin Neurobiol. 2007; 17:593–600. [PubMed: 18093824]
5. Bloom JD, et al. Evolving strategies for enzyme engineering. Curr Opin Struct Biol. 2005; 15:447–452. [PubMed: 16006119]
6. Li QS, Schwaneberg U, Fischer P, Schmid RD. Directed evolution of the fatty-acid hydroxylase P450 BM-3 into an indole-hydroxylating catalyst. Chemistry (Easton). 2000; 6:1531–1536.
7. Glieder A, Farinas ET, Arnold FH. Laboratory evolution of a soluble, self-sufficient, highly active alkane hydroxylase. Nat Biotechnol. 2002; 20:1135–1139. [PubMed: 12368811]
8. Meinhold P, Peters MW, Chen MM, Takahashi K, Arnold FH. Direct conversion of ethane to ethanol by engineered cytochrome P450 BM3. Chem Bio Chem. 2005; 6:1765–1768.
9. Otey CR, Bandara G, Lalonde J, Takahashi K, Arnold FH. Preparation of human metabolites of propranolol using laboratory-evolved bacterial cytochromes P450. Biotechnol Bioeng. 2006; 93:494–499. [PubMed: 16224788]
10. Knutson B, Gibbs SE. Linking nucleus accumbens dopamine and blood oxygenation. Psychopharmacology (Berl). 2007; 191:813–822. [PubMed: 17279377]
11. Schultz W. Multiple dopamine functions at different time courses. Annu Rev Neurosci. 2007; 30:259–288. [PubMed: 17600522]
12. Hyman SE, Malenka RC, Nestler EJ. Neural mechanisms of addiction: the role of reward-related learning and memory. Annu Rev Neurosci. 2006; 29:565–598. [PubMed: 16776597]
13. Damier P, Hirsch EC, Agid Y, Graybiel AM. The substantia nigra of the human brain. II. Patterns of loss of dopamine-containing neurons in Parkinson's disease. Brain. 1999; 122:1437–1448. [PubMed: 10430830]
14. Young AM, Joseph MH, Gray JA. Increased dopamine release *in vivo* in nucleus accumbens and caudate nucleus of the rat during drinking: a microdialysis study. Neuroscience. 1992; 48:871–876. [PubMed: 1378576]
15. Garris PA, Wightman RM. Different kinetics govern dopaminergic transmission in the amygdala, prefrontal cortex, and striatum: an *in vivo* voltammetric study. J Neurosci. 1994; 14:442–450. [PubMed: 8283249]
16. Gubernator NG, et al. Fluorescent false neurotransmitters visualize dopamine release from individual presynaptic terminals. Science. 2009; 324:1441–1444. [PubMed: 19423778]

17. Lindsey KP, Gatley SJ. Applications of clinical dopamine imaging. Neuroimaging Clin N Am. 2006; 16:553–573. [PubMed: 17148019]
18. Ewing AG, Bigelow JC, Wightman RM. Direct *in vivo* monitoring of dopamine released from two striatal compartments in the rat. Science. 1983; 221:169–171. [PubMed: 6857277]
19. Michael AC, Ikeda M, Justice JB Jr. Mechanisms contributing to the recovery of striatal releasable dopamine following MFB stimulation. Brain Res. 1987; 421:325–335. [PubMed: 3500755]
20. Duong TQ, Kim DS, Ugurbil K, Kim SG. Spatiotemporal dynamics of the BOLD fMRI signals: toward mapping submillimeter cortical columns using the early negative response. Magn Reson Med. 2000; 44:231–242. [PubMed: 10918322]
21. Munro AW, et al. P450 BM3: the very model of a modern flavocytochrome. Trends Biochem Sci. 2002; 27:250–257. [PubMed: 12076537]
22. Macdonald ID, Munro AW, Smith WE. Fatty acid-induced alteration of the porphyrin macrocycle of cytochrome P450 BM3. Biophys J. 1998; 74:3241–3249. [PubMed: 9635777]
23. Ravichandran KG, Boddupalli SS, Hasermann CA, Peterson JA, Deisenhofer J. Crystal structure of hemoprotein domain of P450BM-3, a prototype for microsomal P450's. Science. 1993; 261:731–736. [PubMed: 8342039]
24. Modi S, et al. NMR studies of substrate binding to cytochrome P450 BM3: comparisons to cytochrome P450 cam. Biochemistry. 1995; 34:8982–8988. [PubMed: 7619797]
25. Lewis, DFV. Guide to Cytochrome P450 Structure and Function. Taylor & Francis; New York: 2001.
26. Fasan R, Chen MM, Crook NC, Arnold FH. Engineered alkane-hydroxylating cytochrome P450(BM3) exhibiting nativelike catalytic properties. Angew Chem Int Edn Engl. 2007; 46:8414–8418.
27. Bloom JD, Labthavikul ST, Otey CR, Arnold FH. Protein stability promotes evolvability. Proc Natl Acad Sci USA. 2006; 103:5869–5874. [PubMed: 16581913]
28. Ohnuma K, Hayashi Y, Furue M, Kaneko K, Asashima M. Serum-free culture conditions for serial subculture of undifferentiated PC12 cells. J Neurosci Methods. 2006; 151:250–261. [PubMed: 16169086]
29. Ewing AG, Wightman RM, Dayton MA. *In vivo* voltammetry with electrodes that discriminate between dopamine and ascorbate. Brain Res. 1982; 249:361–370. [PubMed: 6814706]
30. Gerhardt GA, Rose GM, Hoffer BJ. Release of monoamines from striatum of rat and mouse evoked by local application of potassium: evaluation of a new *in vivo* electrochemical technique. J Neurochem. 1986; 46:842–850. [PubMed: 3950610]
31. Chen ZJ, et al. A realistic brain tissue phantom for intraparenchymal infusion studies. J Neurosurg. 2004; 101:314–322. [PubMed: 15309925]
32. Michael AC, Ikeda M, Justice JB Jr. Dynamics of the recovery of releasable dopamine following electrical stimulation of the medial forebrain bundle. Neurosci Lett. 1987; 76:81–86. [PubMed: 3495755]
33. Vykhodtseva N, McDannold N, Hynynen K. Progress and problems in the application of focused ultrasound for blood-brain barrier disruption. Ultrasonics. 2008; 48:279–296. [PubMed: 18511095]
34. Li H, Poulos TL. The structure of the cytochrome p450BM-3 haem domain complexed with the fatty acid substrate, palmitoleic acid. Nat Struct Biol. 1997; 4:140–146. [PubMed: 9033595]

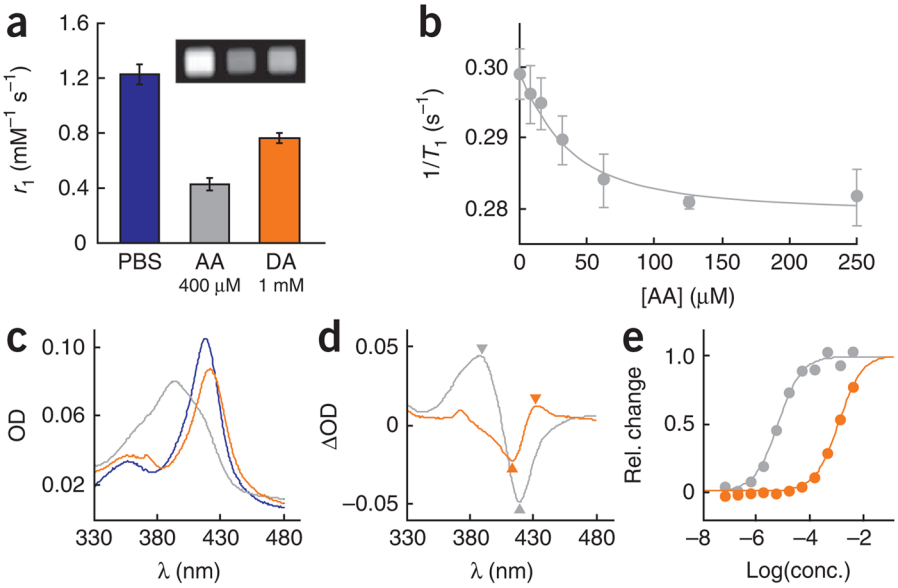

Figure 1.

Ligand binding to the BM3 heme domain changes MRI contrast and optical absorption in a concentration-dependent manner. (**a**) T_1 relaxivity (r_1) of BM3h in PBS solution and in the presence of 400 μM arachidonic acid (AA) or 1 mM dopamine (DA); inset shows T_1-weighted spin echo MRI image intensity (TE/TR = 10/477 ms) of microtiter plate wells containing 240 μM BM3h in PBS alone (left) or in the presence of 400 μM arachidonic acid (middle) or 1 mM dopamine (right). (**b**) T_1 relaxation rates ($1/T_1$) measured from solutions of 28.5 μM BM3h incubated with 0–250 μM arachidonic acid. (**c**) Optical absorbance spectra of 1 μM BM3h measured alone (blue) and after addition of 400 μM arachidonic acid (gray) or 1 mM dopamine (orange). OD, optical density. (**d**) Difference spectra showing the change in BM3h absorbance as a function of wavelength upon addition of 400 μM arachidonic acid (gray) or 1 mM dopamine (orange). (**e**) Normalized titration curves showing binding of BM3h to arachidonic acid (gray) or dopamine (orange). We computed the optical signals used for titration analysis by subtracting the minimum from the maximum of difference spectra (arrowheads in **d**) under each set of conditions. Error bars in **a**, **b** and **e** reflect s.e.m. of three independent measurements (errors in **e** were smaller than the symbols).

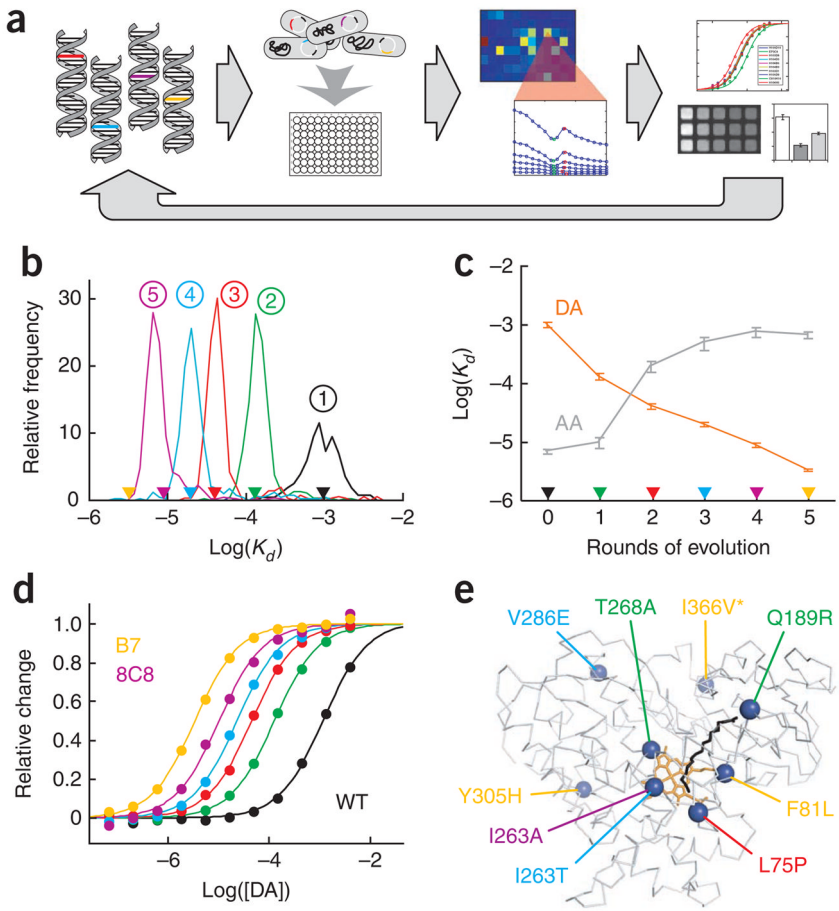

Figure 2.

Screen-based isolation of BM3h mutants with enhanced dopamine affinity. (**a**) Schematic of the directed evolution approach, including (left to right) generation of a mutant DNA library, transformation into *E. coli* and growth in multiwell plate format, spectroscopic analysis of each mutant's ligand binding affinities, and detailed MRI and optical characterization of selected mutant proteins. (**b**) Histograms of mutant dopamine dissociation constants determined during each round of directed evolution, comparing each mutant protein's relative dopamine affinity (measured in plate format) to the K_d of the parent protein (measured in bulk). K_d distributions for screening rounds 1 (black), 2 (green), 3 (red), 4 (cyan) and 5 (purple) are labeled with numbers in circles. Color-coded arrowheads indicate the measured K_ds of parent proteins used to create the library of mutants at each round; yellow arrowhead indicates the K_d of the mutant protein selected after round 5. (**c**) Dissociation constants for dopamine (DA; orange) and arachidonic acid (AA; gray) for WT BM3h and mutant BM3h variants isolated at each round of screening; progressive increases in dopamine affinity and attenuation of arachidonic acid affinity are evident. Colored arrowheads indicate correspondence with data in **b**. Error bars denote s.e.m. of three independent measurements. (**d**) Titration analysis of dopamine binding to WT BM3h and to proteins selected after each round of directed evolution (colored as in **b**). Mutant proteins identified by rounds 4 (8C8) and 5 (B7) were considered to be end products of the screening procedure. (**e**) X-ray crystal structure[34] of WT BM3h (gray; heme group shown in orange) bound to palmitoleic acid (black), indicating the locations of amino acid substitutions accumulated during directed evolution of enhanced dopamine binding affinity. Each mutation's location is marked with a blue sphere and a label color-coded according to the

parent protein in which the substitution was first identified (see legend for **b**). The previously characterized I366V mutation (asterisk) was incorporated between screening rounds 4 and 5 to improve the thermostability of the engineered proteins.

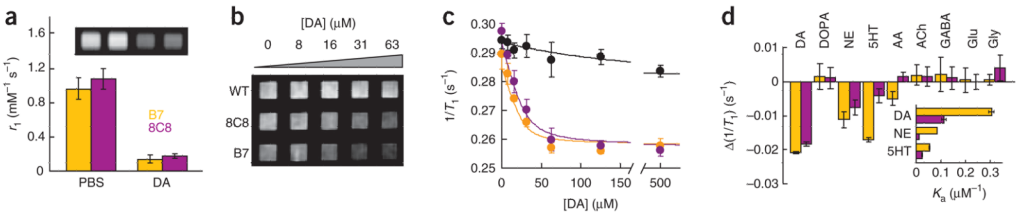

Figure 3.

Selected sensor proteins produce strong and specific MRI signal changes in response to dopamine. (**a**) Relaxivity values measured from BM3h-B7 (yellow bars) and BM3h-8C8 (purple bars) in PBS alone or in the presence of 400 μM dopamine (DA). Inset, T_1-weighted MRI signal (TE/TR = 10/477 ms) obtained from 195 μM BM3h-B7 or BM3h-8C8, each incubated in microtiter plate wells with or without 400 μM dopamine (wells ordered left to right as in the bar graph). (**b**) MRI image showing signal amplitudes measured from wells containing 28.5 μM WT BM3h, BM3h-8C8 or BM3h-B7, each incubated with increasing dopamine concentrations (0–63 μM, left to right). The image was obtained using a T_1-weighted pulse sequence (TE/TR = 10/477 ms). (**c**) Relaxation rates ($1/T_1$ values) measured from solutions of 28.5 μM WT BM3h (black), BM3h-B7 (yellow) or BM3h-8C8 (purple), as a function of total dopamine concentration. Curves were fitted using a ligand-depleting bimolecular association model. (**d**) Changes in $1/T_1$ relative to ligand-free protein for 28.5 μM BM3h-B7 (yellow) or BM3h-8C8 (purple) incubated with 30 μM dopamine, serotonin (5HT), norepinephrine (NE), DOPA, arachidonic acid (AA), acetylcholine (ACh), GABA, glutamate or glycine. Inset, spectroscopically determined affinities ($K_a = 1/K_d$) of BM3h-B7 and BM3h-8C8 for dopamine, serotonin and norepinephrine. Error bars in panels **a**, **c** and **d** denote s.e.m. of three independent measurements.

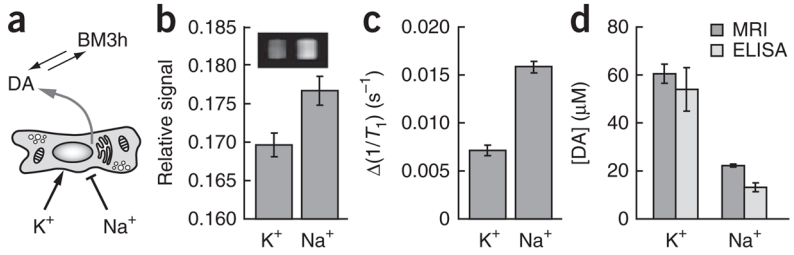

Figure 4.

BM3h-based sensors measure dopamine release in cell culture. (**a**) PC12 cells depolarized by addition of 54 mM K^+ were stimulated to release dopamine (DA) into supernatants containing a BM3h-based sensor; cells did not release dopamine after addition of 54 mM Na^+. (**b**) T_1-weighted spin echo MRI signal amplitudes (TE/TR = 10/477 ms) measured from the supernatants of PC12 cells incubated with 32 μM BM3h-B7 in the presence of K^+ (stimulus) or Na^+ (control). Inset, MRI image of microtiter wells under corresponding conditions. (**c**) Relaxation rates measured from the samples in **b**, minus the relaxation rate of buffer not containing BM3h-based sensors. Given the approximate concentration of BM3h variants in these samples, the $\Delta(1/T_1)$ values presented here can be converted to apparent relaxivities of 0.23 and 0.50 mM^{-1} s^{-1} in K^+ and Na^+ incubation conditions, respectively. (**d**) Data from **c** were used to estimate the concentrations of dopamine present in samples treated with K^+ and Na^+ (dark bars). We independently measured the concentrations of dopamine under equivalent conditions using ELISA (light bars).

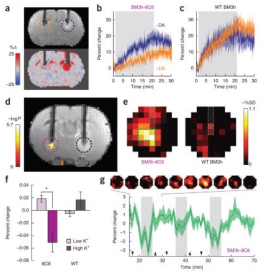

Figure 5.

BM3h-8C8 reports dopamine in injected rat brains. (**a**) Top, coronal MRI image (0.7 mm anterior to bregma, averaged over the injection period) from a single rat injected with 500 μM BM3h-8C8 in the presence (orange dashed circle) or absence (blue dashed circle) of equimolar dopamine; the image contrast was linearly adjusted for display. MRI hyperintensity is noticeable near the tip of the dopamine-free cannula. The circles indicate approximate ROIs (~1.5 mm around cannula tips) over which image intensity was averaged for quantitative analyses. Bottom, map of percent signal change (%Δ) for the same animal, computed by comparing pre- and post-injection MRI signal. Areas corresponding to both high- and low-dopamine co-injections (+DA and −DA) are delineated by apparent signal changes, but the strong difference between the two conditions is clear. (**b**) Time courses of relative signal change observed during injection of BM3h-8C8 −DA (blue) or +DA (orange), averaged over multiple animals (n = 7) in ROIs denoted in **a**. Gray shading denotes the 20-min injection period. (**c**) Corresponding time courses of a control injection in which WT BM3h was introduced instead of the dopamine sensor (n = 5). (**d**) Statistical parametric map of t-test significance values (color scale) for correlation of MRI intensity with low- and high-K^+ conditions in an individual rat, overlaid on a corresponding T_1-weighted coronal slice (grayscale) showing injection cannulae used for BM3h-8C8 infusion (left, purple dashed circle) and WT BM3h control infusion (right, black dashed circle). (**e**) Maps of percent signal difference (SD) between high- and low-K^+ conditions observed in 2.7-mm-diameter ROIs centered around BM3h-8C8 sensor (left) and WT BM3h control (right) injection sites, after spatial coregistration and averaging across multiple animals (n = 6); ROIs correspond approximately to the color-coded circles in **d**. Voxels outlined in green are those that showed the most significant correlation with the K^+ stimulus regressor in the group analysis (Student's t-test, $P < 0.01$); these generally showed ~1% mean signal change. Gray cross-hatching indicates approximate locations of the infusion cannulae. (**f**) Mean MRI signal change from baseline observed during high-K^+ (dark bars) and low-K^+ (light bars) periods in ROIs centered around infusion sites for BM3h-8C8 (purple) and WT BM3h (gray) proteins. ROIs were cylinders 2.7 mm in diameter and extending over three 1-mm-thick slices registered around the infusion sites; signal was averaged in unbiased fashion over all voxels, regardless of correlation with the stimulus. The signal difference in the presence of BM3h-8C8 was statistically significant (P = 0.0008, asterisk). (**g**) Graph shows the mean time course of MRI signal in voxels within the BM3h-8C8–infused ROI and identified as correlated ($P < 0.05$) with the stimulus, averaged over animals and binned over 1.5-min intervals (shaded area denotes s.e.m., n = 6; individual traces are shown in Supplementary Fig. 6 online). Gray vertical bars denote periods associated with highest K^+ stimulation, accounting for delays due to convective spreading of K^+ from the cannulae tips and the dead time of the injection apparatus. Arrowheads indicate the timing of pump switches associated with transitions from low to high (up) and from high to low (down) K^+ infusion conditions. Panels above the graph depict 'snapshots' of signal change spaced throughout the first K^+ stimulation cycle, as indicated by the dotted lines. The ROI corresponds to the left side of **e**, and the color scale denotes 0% (black) to 3% (yellow) signal change from baseline at each voxel and time point.